

Spectro-spatial wave features in nonlinear metamaterials: Theoretical and computational studies

Mohammad Bukhari^a, Eshagh Farzaneh Joubaneh^a, Oumar Barry^{a,*}

^a*Department of Mechanical Engineering, Virginia Tech, Blacksburg, VA, 24061, USA*

Abstract

Considerable attention has been given to nonlinear metamaterials because they offer some interesting phenomena such as solitons, frequency shifts, and tunable bandgaps. However, only little is known about the spectro-spatial properties of a wave propagating in nonlinear periodic chains, particularly, a cell with multiple nonlinear resonators. This problem is investigated here. Our study examines both hardening and softening nonlinearities in the chains and in the local resonators. Explicit expressions for the nonlinear dispersion relations are derived by the method of multiple scales. We validate our analytical results using numerical simulations. The numerical simulation is based on spectro-spatial analysis using signal processing techniques such as spatial-spectrogram and wave filtering. The spectro-spatial analysis provides detailed information about the interactions of dispersive and nonlinear phenomena of waveform in both short and long-wavelength domains. Furthermore, we validate and demonstrate the theoretically obtained bandgaps, wave distortion, and birth of solitary

*Corresponding author

Email addresses: bukhari@vt.edu (Mohammad Bukhari), farza1e@cmich.edu (Eshagh Farzaneh Joubaneh), obarry@vt.edu (Oumar Barry)

waves through a computational study using finite element software, ANSYS. The findings, in both theoretical and computational analyses, suggest that nonlinear resonators can have more effect on the waveform than the nonlinear chains. This observation is valid in both short and long wavelength limits.

1. INTRODUCTION

Introducing unique dynamic properties artificially from engineering configurations and material constituent leads to promising materials with exceptional characteristics in different engineering applications. These materials, which are called metamaterials, have attracted many researchers because of their wider applications in different fields. They were first introduced in electromagnetic and optical wave propagation and later extended to mechanical waves applications[1, 2].

Mechanical metamaterials are often fabricated from periodic cells arranged carefully. The earliest study of periodic structure was in the 1900s [3–8]. These structures form bandgaps due to Bragg scattering at wavelengths near their lattice constant. This enables, for example, vibration attenuation at low frequencies located inside the bandgap. However, the condition associated with Bragg scattering makes this application limited to large structures.

Attaching local resonators on the crystal allows a bandgap formation at wavelengths much larger than the lattice constant [9]. This enables the vibration control of small structures at low frequencies, thus widening the possible applications of metamaterials. Further investigation on the comparison between

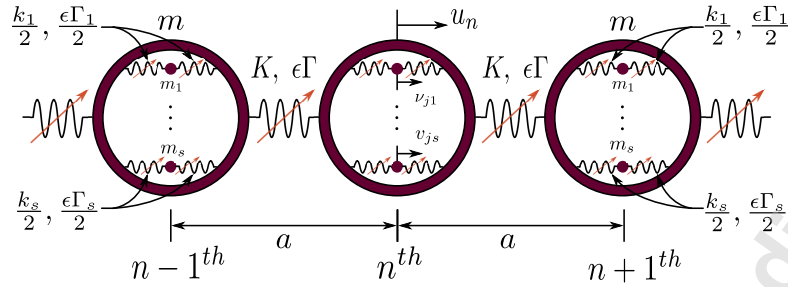


Figure 1: A schematic diagram for the nonlinear acoustics metamaterial

local resonator and Bragg scattering concepts can be found in [10]. Multiple bandgaps at different frequency ranges can also be developed by using multiple resonators with different parameters [11, 12].

Beyond vibration suppression, nonlinear metamaterials offer a wide pool of applications including gap solitons [13], dark solitons, envelope and dark solitons [14], wave non-reciprocity [15], and altering band structure limits [16].

Weakly nonlinear acoustics metamaterials were investigated analytically by using different perturbation techniques [17, 18]. For instance, Narisetti et al. [19], employed the Lindstedt-Poincare method in deriving the dispersion relations for nonlinear chain and validated the results numerically. The method of multiple scales can deal with more complicated nonlinear systems like multiple waves interaction or nonlinear resonators [20, 21].

Early considerations of nonlinear continuum phononic media can be found in [22, 23]. Furthermore, enhancing the vibration attenuation performance can be realized using chains with two coupled nonlinear resonators [24, 25].

Wave non-reciprocity can be used in uni-directional acoustic wave propagation (e.g. acoustics diode). This can be obtained by coupling linear and

nonlinear mediums [15, 26, 27], bifurcation in granular structures [28], or nonlinear hierarchical internal structures [29]. Moreover, an acoustic rectifier can be obtained by a cubic weakly nonlinear oscillator attached to a linear periodic lattice such that the operation frequencies of the rectifier coincide with the secondary resonances of the nonlinear oscillator [30].

Analyzing nonlinear metamaterials is often performed by tracking the change in the temporal state properties and discussing the existence of solitary waves, and dispersion characteristics. However, Ganesh and Gonella [31] have studied the spectro-spatial wave packet propagation features of nonlinear periodic chains by utilizing some signal processing tools. This allows detecting wave localization (birth of solitons), and reconstructing dispersion curves. However, although their analytical expressions could predict the shift in dispersion curves, many other nonlinear phenomena could not be inferred. Zhou et al. [32], extended Ganesh and Gonella's work by including local linear resonators and studying the spectro-spatial wave features of nonlinear acoustic metamaterial. In both studies [31, 32], the effect of nonlinearity in the chain was limited to short wavelength region only. None of the studies included the nonlinearity in local resonators or determined how nonlinear resonators affect dispersion characteristics or propagation of solitary waves in both long and short-wavelength domains. None of the past works included the nonlinearity in the local resonators to study their effect on the wave propagation in both long and short-wavelength domains. The goal of the current study is to fill this knowledge gap by studying a nonlinear metamaterial consisting of nonlinear chains with multiple local resonators.

The present study is performed using different analytical and computational techniques in order to show the ability of obtaining interesting nonlinear wave propagation phenomena at all wavelength limits.

Seeking a nonlinear system that offers interesting wave propagation phenomena in all wavelength regions, which is a rare find, we recently investigated the nonlinear vibration of a nonlinear chain with multiple nonlinear local resonators analytically and numerically [33–35]. In order to validate the observed nonlinear wave propagation features, we extend our conference paper in [35] by reporting a thorough theoretical and computational studies. The nonlinearity is assumed to be weakly cubic type with softening or hardening nonlinear coefficients. In one case, we study the effect of nonlinearity attributed to the nonlinearity in the chain only. In another case, we examine the nonlinearity effect caused by the local resonator only. We employ the method of multiple scales to generate approximate close form expressions for the dispersion curves of a nonlinear (or linear) chain with any number of linear (or nonlinear) resonators. We follow this by numerical simulations of the metamaterial subjected to a wave packet input impulse. The results are used to check our analytical model in predicting the cut-off frequency. We then use multiple signal processing tools in order to investigate the spectro-spatial properties of the nonlinear acoustic metamaterial. Furthermore, we study the effect of both hardening and softening nonlinearities in the chain and in the local resonators. Finally, we conduct a computational study using finite element software ANSYS to validate the bandgaps, birth of solitary waves, and other spectro-spatial properties. The findings suggest that

very interesting dispersion characteristics and propagation of solitary wave can be realized in both long-wavelength and short-wavelength domains using nonlinear chain with multiple nonlinear local resonators. These interesting wave propagation characteristics can be employed to design superior vibration isolation and acoustic diode devices.

The remainder of the paper is organized as follows. The next section describes the system of interest and presents explicit expressions for the nonlinear dispersion relations. The obtained analytical expressions are validated through direct numerical simulations and results from the literature. Spectro-spatial analysis is then carried out to explain the relation between topological/physical (space-time domain) and spectral domains. Finally, we present a computational study using ANSYS to further validate and demonstrate the interesting wave characteristics observed from the analytical and numerical results. Our findings are then summarized in the conclusion.

2. SYSTEM DESCRIPTION AND MATHEMATICAL MODELING

A schematic diagram for the acoustic metamaterial chain is depicted in Fig. 1. The chain consists of periodic cells. Each cell is represented by a mass, m , and it is connected to the other cells by a linear or nonlinear spring with linear coefficient, k , and nonlinear coefficient $\epsilon\Gamma$. There are s number of local resonators in each cell. The i^{th} resonator consists of a mass, m_i and connected to the n^{th} cell by a linear or nonlinear spring with linear coefficient, k_i , and a nonlinear coefficient, $\epsilon\Gamma_i$. It is noteworthy here that the system is reduced to a

linear system if $\epsilon = 0$.

The equations of motion for the n^{th} cell can be expressed as follows [19, 32]

$$\begin{aligned}
 & m\ddot{u}_n + K(2u_n - u_{n-1} - u_{n+1}) + \\
 & \epsilon\Gamma((u_n - u_{n-1})^3 + (u_n - u_{n+1})^3) + \\
 & \sum_{i=1}^s k_i(u_n - v_{ni}) + \sum_{i=1}^s \epsilon\Gamma_i(u_n - v_{ni})^3 = 0
 \end{aligned} \tag{1}$$

$$m_i\ddot{v}_{ni} + k_i(v_{ni} - u_n) + \epsilon\Gamma_i(v_{ni} - u_n)^3 = 0 \tag{2}$$

For the case of nonlinear chain only, we set $\Gamma_i = 0$ while we set $\Gamma = 0$ in the case of nonlinear resonator only.

Eqns. (1)-(2) can be written in the non-dimensional form as

$$\begin{aligned}
 & \ddot{u}_n + 2u_n - u_{n-1} - u_{n+1} + \epsilon\bar{\Gamma}((u_n - u_{n-1})^3 + \\
 & (u_n - u_{n+1})^3) + \sum_{i=1}^s \bar{k}_i(u_n - v_{ni}) + \sum_{i=1}^s \epsilon\bar{\Gamma}_i(u_n - v_{ni})^3 = 0
 \end{aligned} \tag{3}$$

$$\frac{\omega_n^2}{\omega_{di}^2} \ddot{v}_{ni} + (v_{ni} - u_n) + \epsilon\bar{\Gamma}_i(v_{ni} - u_n)^3 = 0 \tag{4}$$

where the dots here denote the derivative in terms of the non-dimensional time

$$\tau = \omega_n t, \bar{\Gamma} = \frac{\Gamma}{\omega_n^2 m}, \bar{k}_i = \frac{k_i}{\omega_n^2 m}, \omega_n^2 = K/m, \text{ and } \omega_{di}^2 = k_i/m_i.$$

2.1. Approximate Analytical Solution by the Method of Multiple Scales

For weakly nonlinear systems like the one presented in Eqns. (3)-(4), perturbation techniques can be employed to obtain approximate analytical solution of the dispersion curves. Here we use the method of multiple scales to present explicit expressions for the dispersion relations. The method of multiple scales

is advantageous over other techniques due to the simplicity of handling and collecting the secular terms in multiple equations or complicated systems. The approximate solution can be represented up to second order approximation as [18]

$$u_n(t, \epsilon) = u_{n0}(T_0, T_1) + \epsilon u_{n1}(T_0, T_1) \quad (5)$$

$$v_{ni}(t, \epsilon) = v_{ni0}(T_0, T_1) + \epsilon v_{ni1}(T_0, T_1) \quad (6)$$

where $T_0 = \tau$ is the fast time scale and $T_1 = \epsilon\tau$ is the slow time scale. The system can now be represented by two independent variables (scales) and applying the full derivative is not valid any more. Instead, we can represent the time derivative by the chain rule as

$$(\ddot{}) = D_0^2 + 2\epsilon D_0 D_1 + \dots \quad (7)$$

where $D_n = \frac{\partial}{\partial T_n}$.

Using Bloch theory for infinite periodic medium [36] (also known as Floquet theory for 1-dimensional medium [37]), the solution of the linear system can be expressed as

$$u_n = A e^{j(n\bar{k} - \omega T_0)} + c.c \quad (8)$$

$$v_{ni} = B_i e^{j(n\bar{k} - \omega T_0)} + c.c \quad (9)$$

where $\bar{k} = aq$ is the nondimensional wavenumber, and $c.c$ is the complex conjugate. For convenience, we drop the bar from \bar{k} in the subsequent analysis since the linear stiffness of the chain k does not appear any more in the normalized

parameters.

Substituting Eqns. (5)-(7) into Eqns. (3)-(4), collecting the coefficients of ϵ^0 & ϵ , and then substituting Eqns. (8)-(9), one can write the linear dispersion relation for all cases of nonlinearity as

$$-\omega^2 + (2 - 2 \cos k) + \sum_{i=1}^s \bar{k}_i (1 - K_{\omega i}) = 0 \quad (10)$$

where $K_{\omega i} = \frac{1}{1 - \omega_n^2 \omega^2 / \omega_{di}^2}$. To derive the nonlinear solution, the vibration amplitude should be written in the polar form as

$$A = \frac{1}{2} \alpha e^{i\beta} \quad (11)$$

Solving for the amplitude α , reveals that $\alpha = \alpha_0$, where α_0 is a constant, for both cases of nonlinearity. The phase can be written for each case as [34?]

- Nonlinear chain $\bar{\Gamma} \neq 0$

$$\beta = -\frac{3\bar{\Gamma}\alpha^2(1 - \cos k)^2}{2\omega(1 + \sum_{i=0}^s \frac{\bar{k}_i \omega_n^2 / \omega_{di}^2}{1 - \omega_n^2 \omega^2 / \omega_{di}^2} K_{\omega i})} T_1 \quad (12)$$

- Nonlinear resonator $\bar{\Gamma}_i \neq 0$

$$\beta = -\frac{\sum_{i=1}^s [\frac{3}{8}\alpha^2(1 - K_{\omega i})^3 \bar{\Gamma}_i (\frac{\bar{k}_i}{1 - \omega_n^2 \omega^2 / \omega_{di}^2} - 1)]}{\omega(1 + \sum_{i=1}^s \frac{\bar{k}_i \omega_n^2 / \omega_{di}^2}{1 - \omega_n^2 \omega^2 / \omega_{di}^2} K_{\omega i})} T_1 \quad (13)$$

Therefore, the nonlinear dispersion curves can be written as

$$\omega_{nl} = \omega + \epsilon\beta' \quad (14)$$

where β' is the derivative in terms of the slow time scale.

From Eqn. (12), it can be observed that the nonlinear frequency in the nonlinear chain case is a function of wavenumber. In fact, the correction factor $\beta \sim 0$ when k is very small and hence the effect of chain nonlinearity (β) is negligible for long wavelength limit ($k \sim 0$) at both acoustic and optical modes. On the other hand, for the case of the nonlinear resonator (Eqn. (13)), the wavenumber does not explicitly appear in the expression of the correction factor and hence the only wavenumber dependence in this case is through the linear dispersion relation (i.e. Eqn. (10)). Also note the appearance of a new term $(1 - K_{\omega_i})^3$ in the numerator of Eqn. (13), which can have a significant effect on the correction factor β and hence on the nonlinear frequency when the resonator is tuned to the excitation frequency regardless of the wavenumber. It is noteworthy here that the derived expression for, β in Eqn. (13), is correct and different from that obtained in [16], since the latter omitted the contribution of the resonators on the left hand side from the equations at order ϵ [19, 20] (for more information refer to [38]).

3. VALIDATING ANALYTICAL RESULTS

To validate the dispersion relations obtained by the method of multiple scale, we compare the current results with those obtained in the literature for a nonlinear chain single linear resonator system obtained by Lindstedt-Poincare methods and with those obtained numerically. For this part, we select $\omega_n = \omega_{d1} = 1000$ rad/sec, $\bar{k}_i = 1$, $s = 1$, $\epsilon \bar{\Gamma} \alpha^2 = 0.06$, and $\epsilon \bar{\Gamma}_i \alpha^2 = 0$.

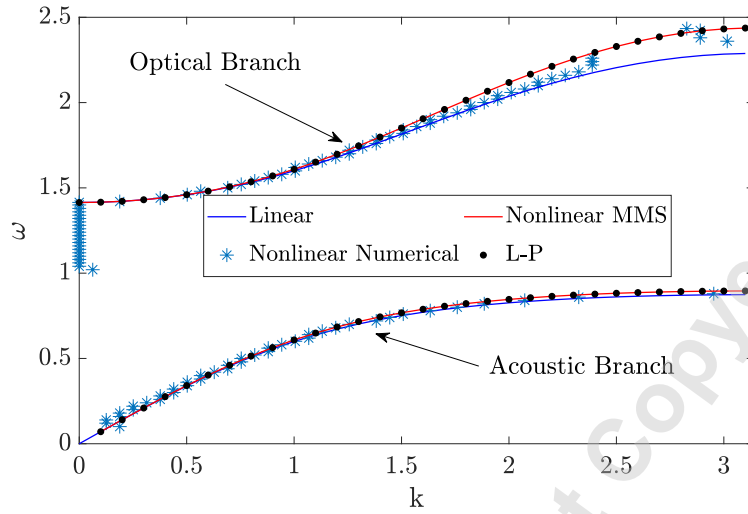


Figure 2: Validating the results of nonlinear chain with single linear resonator, $\epsilon \bar{\Gamma} \alpha^2 = 0.06$, $\epsilon \bar{\Gamma}_1 \alpha^2 = 0$.

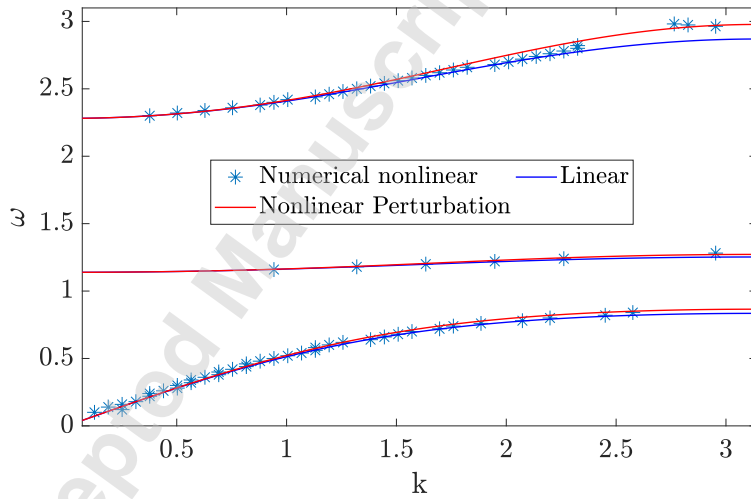


Figure 3: Validating the results of nonlinear chain with two linear resonators, $\epsilon \bar{\Gamma} \alpha^2 = 0.06$, $\epsilon \bar{\Gamma}_1 \alpha^2 = \epsilon \bar{\Gamma}_2 \alpha^2 = 0$.

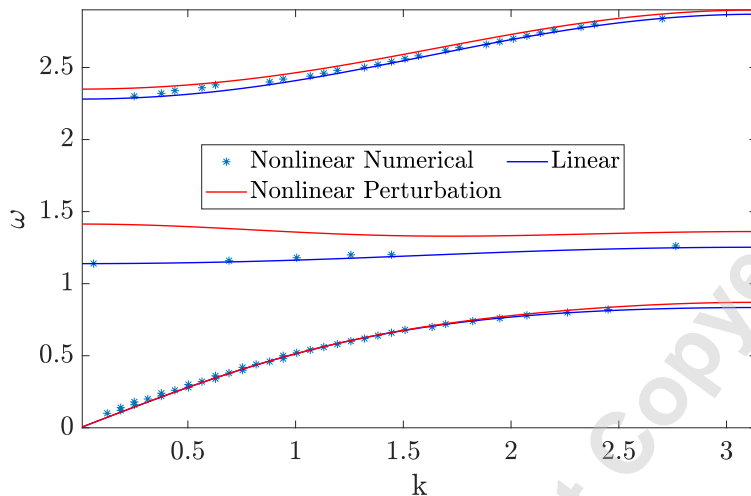


Figure 4: Validating the results of linear chain with two nonlinear resonators, $\epsilon\bar{\Gamma}\alpha^2 = 0$, $\epsilon\bar{\Gamma}_1\alpha^2 = 0.06$, $\epsilon\bar{\Gamma}_2\alpha^2 = 0$.

For numerical simulations, we simulate a chain consisting of 500 cells and attached to it s number of resonators (e.g. $s = 1$ in the first part of the validation, then we set $s = 2$). The boundaries of the chain are assumed to be a perfectly matched layer (PML) in order to absorb and dissipate incoming waves, as well as, to minimize wave reflections at each end [19]. The system is excited by a transient wave packets signal at different wavenumbers. The velocity of the wave packet is selected to limit the motion of the signal in one direction and suppress any waves traveling in the opposite direction [31]. The numerical integration is carried out using MATLAB built in integrator ODE45 (Runge-Kutta). After running the simulation at a specific wavenumber, 2-D Fast Fourier Transform is applied on the displacement matrix and the frequency and wavenumber corresponding to the maximum amplitude value are collected.

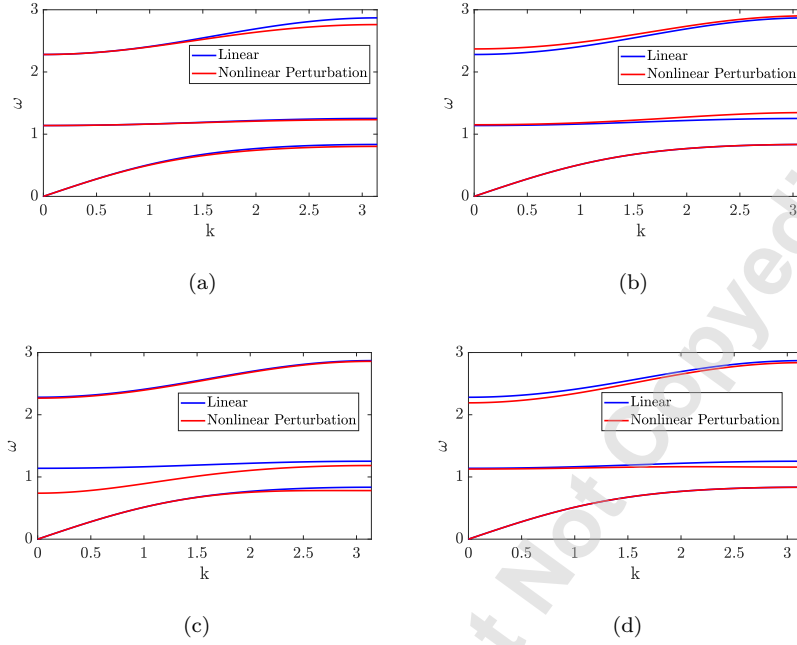


Figure 5: Analytical dispersion curves for acoustics metamaterial and two local resonators with different types and sources of nonlinearities: (a) Softening chain nonlinearity $\epsilon\bar{\Gamma}\alpha^2 = -0.06$, $\epsilon\bar{\Gamma}_1\alpha^2 = \epsilon\bar{\Gamma}_2\alpha^2 = 0$; (b) Hardening resonator nonlinearity $\epsilon\bar{\Gamma}_2\alpha^2 = 0.06$, $\epsilon\bar{\Gamma}_1\alpha^2 = \epsilon\bar{\Gamma}\alpha^2 = 0$; (c) Softening resonator nonlinearity $\epsilon\bar{\Gamma}_1\alpha^2 = -0.06$, $\epsilon\bar{\Gamma}\alpha^2 = \epsilon\bar{\Gamma}_2\alpha^2 = 0$; (d) Softening resonator nonlinearity $\epsilon\bar{\Gamma}_2\alpha^2 = -0.06$, $\epsilon\bar{\Gamma}_1\alpha^2 = \epsilon\bar{\Gamma}\alpha^2 = 0$.

These values represent the point in the dispersion curve corresponding to the wavenumber of excitation signal [20]. The wavenumber is then swept to reconstruct other points in the dispersion curves. These wave packets excitation can be defined as:

$$u_m(0) = \frac{1}{2}(H(m-1) - H(m-1 - N_{cy}2\pi/k))(1 - \cos(mk/N_{cy})) \sin(mk) \quad (15)$$

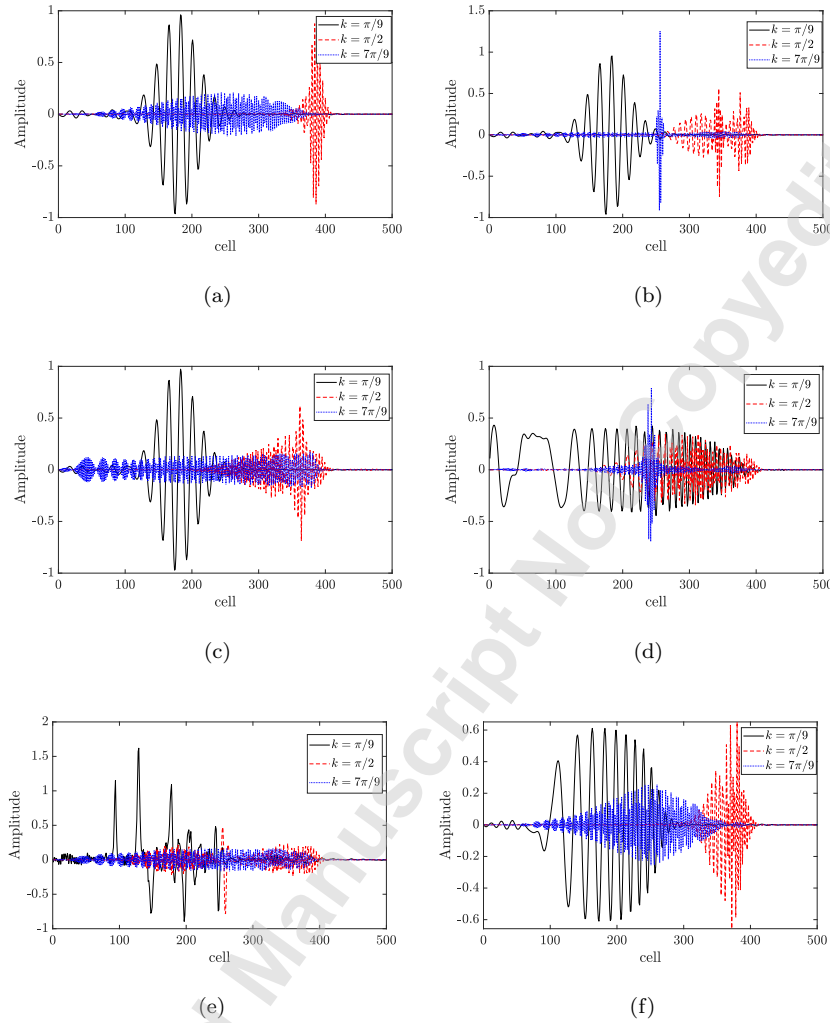


Figure 6: Spatial profile of the wave packet for different types and sources of nonlinearities at frequencies in the upper branch of dispersion curve: (a) Linear chain $\epsilon\bar{\Gamma}\alpha^2 = \epsilon\bar{\Gamma}_1\alpha^2 = \epsilon\bar{\Gamma}_2\alpha^2 = 0$; (b) Hardening chain nonlinearity $\epsilon\bar{\Gamma}\alpha^2 = 0.03$, $\epsilon\bar{\Gamma}_1\alpha^2 = \epsilon\bar{\Gamma}_2\alpha^2 = 0$; (c) Softening chain nonlinearity $\epsilon\bar{\Gamma}\alpha^2 = -0.03$, $\epsilon\bar{\Gamma}_1\alpha^2 = \epsilon\bar{\Gamma}_2\alpha^2 = 0$; (d) Hardening resonator nonlinearity $\epsilon\bar{\Gamma}_2\alpha^2 = 0.03$, $\epsilon\bar{\Gamma}_1\alpha^2 = \epsilon\bar{\Gamma}\alpha^2 = 0$; (e) Softening resonator nonlinearity $\epsilon\bar{\Gamma}_2\alpha^2 = -0.03$, $\epsilon\bar{\Gamma}_1\alpha^2 = \epsilon\bar{\Gamma}\alpha^2 = 0$; (f) Hardening resonator nonlinearity $\epsilon\bar{\Gamma}_1\alpha^2 = 0.03$, $\epsilon\bar{\Gamma}_2\alpha^2 = \epsilon\bar{\Gamma}\alpha^2 = 0$.

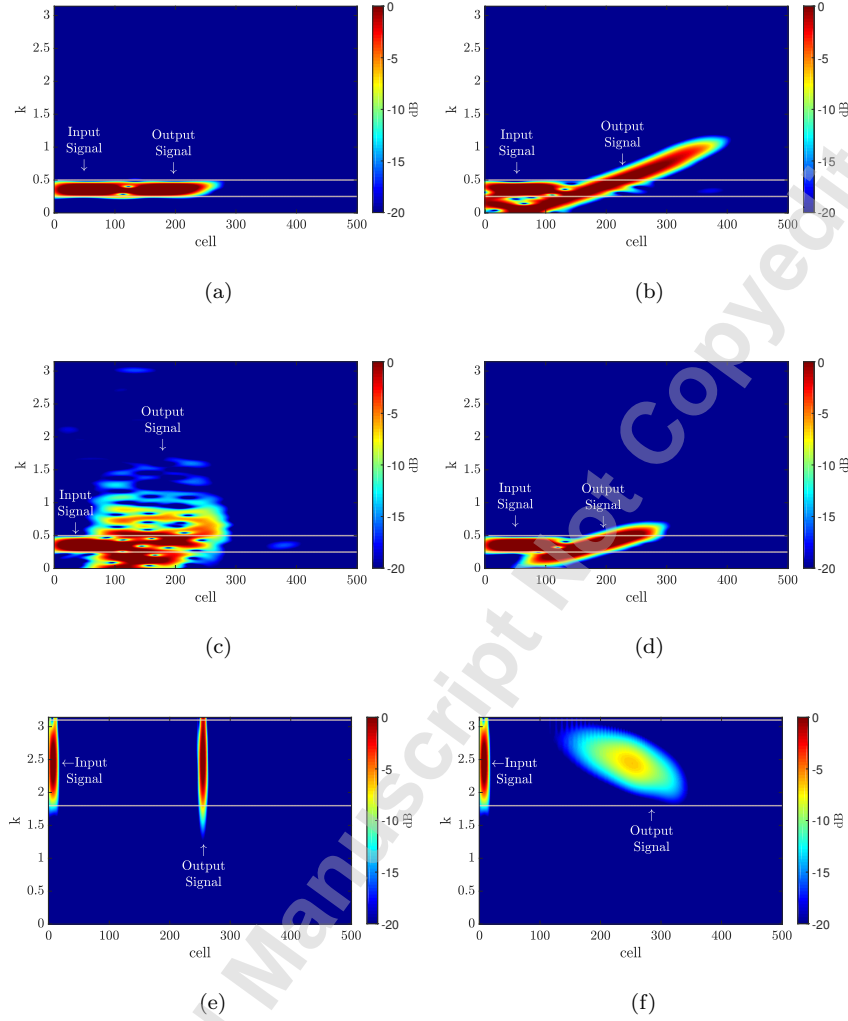


Figure 7: Spatial spectrograms of the wave packet for different types and sources of nonlinearities at frequencies in the upper branch of dispersion curve: (a) Hardening chain nonlinearity $\epsilon\bar{\Gamma}\alpha^2 = 0.03$, $\epsilon\bar{\Gamma}_1\alpha^2 = \epsilon\bar{\Gamma}_2\alpha^2 = 0$, $k = \pi/9$; (b) Hardening resonator nonlinearity $\epsilon\bar{\Gamma}_2\alpha^2 = 0.03$, $\epsilon\bar{\Gamma}_1\alpha^2 = \epsilon\bar{\Gamma}\alpha^2 = 0$, $k = \pi/9$; (c) Softening resonator nonlinearity $\epsilon\bar{\Gamma}_2\alpha^2 = -0.03$, $\epsilon\bar{\Gamma}_1\alpha^2 = \epsilon\bar{\Gamma}\alpha^2 = 0$, $k = \pi/9$; (d) Hardening resonator nonlinearity $\epsilon\bar{\Gamma}_1\alpha^2 = 0.03$, $\epsilon\bar{\Gamma}_2\alpha^2 = \epsilon\bar{\Gamma}\alpha^2 = 0$, $k = \pi/9$; (e) Hardening resonator nonlinearity $\epsilon\bar{\Gamma}_2\alpha^2 = 0.03$, $\epsilon\bar{\Gamma}_1\alpha^2 = \epsilon\bar{\Gamma}\alpha^2 = 0$, $k = 7\pi/9$; (f) Hardening resonator nonlinearity $\epsilon\bar{\Gamma}_1\alpha^2 = 0.03$, $\epsilon\bar{\Gamma}_2\alpha^2 = \epsilon\bar{\Gamma}\alpha^2 = 0$, $k = 7\pi/9$.

$$\begin{aligned} \dot{u}_m(0) = & \frac{1}{2}(H(m-1) - H(m-1 - N_{cy}2\pi/k)) \\ & (-\omega_n\omega/N_{cy} \sin(mk/N_{cy}) \sin(mk) - \omega_n\omega(1 - \\ & \cos(mk/N_{cy})) \cos(mk)) \end{aligned} \quad (16)$$

$$v_{mi}(0) = K_{\omega i} u_m(0) \quad (17)$$

$$\dot{v}_{mi}(0) = K_{\omega i} \dot{u}_m(0) \quad (18)$$

where $H(x)$ is the heaviside function and N_{cy} is the cycles number and set in the current study to $N_{cy} = 7$.

Fig. 2 presents a comparison between our results, the literature results, and the numerical results. Our multiple scales results show very good agreement for the case of nonlinear chain with single linear resonator.

For the case of nonlinear chain with multiple linear resonators, we validate our analytical results using numerical simulation only since the literature lacks simulations for similar nonlinear systems. The results are shown in Fig. 3 for the case of two resonators where $\omega_{d1} = \omega_n$ and $\omega_{d2} = 1.5\omega_n$. The results show that the method of multiple scales can accurately predict, in general, dispersion curves and the trend of this type of nonlinearity. However, it fails to predict any other nonlinear dynamics phenomena such as solitons and the presence of secondary resonances as we will show in the following sections.

Furthermore, the numerical and analytical results of the nonlinear resonator are plotted in Fig. 4. We can observe that the method of multiple scales is a

good predictor of the upper and lower branches of the dispersion curve, but a poor predictor of the middle branch when the natural frequency of the system is $\omega_{d1} = \omega_n$. Therefore, this region should be handled by a different approach.

4. THE EFFECT OF DIFFERENT TYPES OF NONLINEARITIES ON THE BANDGAP BOUNDARIES

After checking the obtained solution for each case, we examine the effect of nonlinearity on the wave propagation in various wavelength regions. In addition to Figs. 3-4, we present the analytical dispersion curves for different kind and source of nonlinearities in Fig. 5.

We can observe from Fig. 3 and Fig. 5.(a) that the nonlinear chain affects mainly the short wavelength region ($k \sim \pi$). The effect of nonlinearity in the long wavelength region ($k \sim 0$) is almost negligible; however, a significant shift of the dispersion curves is observed at high wavenumbers. On the other hand, Fig. 4 and Figs. 5.(b)-(d) show that systems with nonlinear resonators have significant impact on the dispersion curves in the long wavelength region.

Moreover, it is demonstrated that the effect of nonlinear resonators becomes more pronounced at frequencies near the resonator frequency. For instance, in Fig. 4 and Fig. 5.(c), a significant shift occurs near the resonance frequency of the nonlinear resonators $\omega_{d1} = \omega_n$. However, making the second resonators $\omega_{d2} = 1.5\omega_n$ nonlinear, shifts the effect of nonlinearity to other frequency regions.

It is also demonstrated that tuning the bandgap can be done by changing the type of nonlinearity. In Fig. 5.(a) and Figs. 5.(c)-(d), softening nonlinearity

shifts the dispersion curves lower, thus increasing the size of the bandgap. On the other hand, hardening nonlinearity shifts the dispersion curves up as shown in Figs. 3-4 and Fig. 5.(b).

5. SPECTRO-SPATIAL ANALYSIS

Although the cut-off frequencies can be predicted by the method of multiple scales, other nonlinear wave propagation features cannot be characterized. This merits the use of spectro-spatial analysis to characterize the wave propagation in the proposed metamaterial. It should be noted that all the following simulations are based on the optical branch because this branch is more affected by nonlinearity than the acoustic branch. Also the numerical simulation for the optical mode is much faster. Moreover, Figs. 6-7 are plotted at the end of the numerical simulations. The numerical simulations lasted for $t = 8$ sec.

The spatial profile of the wave packet is depicted in Fig. 6 for different types of nonlinearities. For the linear case (Fig. 6 (a)), the output profile of the long wavelength limit is a mirror image of the input signal profile. However, increasing the wavenumber gradually turns the input wave into a dispersive wave (i.e, the output wave get stretched over the chain and the wave amplitude becomes smaller). In addition, we observe that the nonlinear chain gives rise to travelling localized wave (i.e. solitary waves) with increasing wavenumber when the nonlinearity is hardening (Fig. 6.(b)) and wave dispersive (i.e., the wave is stretched over the chain) when the nonlinearity is softening (Fig. 6.(c)). This can be explained by the change in the dispersion curve slope (i.e., see discus-

sions on Fig. 8). For instance, hardening nonlinear chain has a fixed linear slope instead of a variable slope in the dispersion curve. This is an indication of solitary (localized) waves [23]. On the other hand, Figs. 6.(a)-(c) indicate that nonlinear hardening chain has no effect on the wave profile in long wavelength region for both types of nonlinearities (i.e., the input signal has the same profile as the output signal at long wave length region). The opposite is observed in Figs. 6.(d)-(f) when the system is changed to linear chains with nonlinear local resonators. It is evident that the wave profile is distorted in all wavelength domains unlike the nonlinear chain case. In Fig. 6.(d), a hardening resonator exhibits dispersive wave at long wavelength and travelling localized wave at short wavelength. On the other hand, a softening resonator shows an interesting behavior at long wavelength limit since the wave profile has travelling localized and dispersive components. However, the travelling localized component vanishes with reducing wavelength (i.e. increasing wavenumber) as shown in Fig. 6.(e). Therefore, unlike the case of nonlinear chain, wave distortion can be obtained at all wavelength limits in the case of nonlinear resonator. This effect of resonator nonlinearity depends significantly on the frequency of the nonlinear resonator. For example, tuning the nonlinear resonator away from the upper dispersion curve results in significant reduction in the effect of nonlinear wave propagation phenomena, specifically, in the short wavelength region as shown in Fig. 6.(d). It is noteworthy that, albeit the analytical dispersion curves fail to predict the cut-off frequency and other important wave propagation features, they accurately predict how the nonlinearities in both the chains and resonators affect

the wave propagation across all wavelength domains. In that, their predictions about the effect of nonlinearities agree with the spatial profile plots. For example, both Fig. 3 and Fig. 6.(b) show hardening chains to have no effect in long-wavelength domain and significant effect in short wavelength domain.

Fig. 7 shows the spectrograms of the wave propagating through the metamaterial in both short and long-wavelengths. As we observed before, the nonlinear chain has no effect on the structure in the long wavelength limit. This is clearly shown in Fig. 7.(a), the output wave profile is exactly the same as the input signal. However, as shown in Figs. 7.(b)-(c), a significant distortion (i.e., the output wave is split into multiple components and/or there are other forms of deformation resulting from resonator and chain nonlinearity) to the input signal is observed when we change the nonlinearity from chain to local resonator. The signal becomes clearly dispersive (i.e., the output wave get stretched over the chain) along the chain with significant equal amplitude when the nonlinearity is hardening as shown in Fig. 7.(b). When the nonlinearity is of softening type, we observe multiple localized signals, as well as, dispersive components (Fig. 7.(c)). The dispersive components are generated at a wide range of wavenumbers outside the initial signal wavenumber content. In the short wavelength region, the effect of nonlinear resonator is similar to that of nonlinear chain: the output signal is localized unlike in the linear case where the signal at this limit is completely dispersive. As we will show in the below discussions, this indicates that soliton formation is also possible in the case of nonlinear resonator as shown in Fig. 7.(e). In Fig. 7.(d) and Fig. 7.(f), it is observed that a nonlinear resonator

with frequency away from the excitation frequency has less effect on the wave profile, specifically in the short wavelength limit where it is completely linear. Therefore, a properly tuned nonlinear resonator can distort the output wave at all wavelength limits. The output signal appears at frequencies different than the input frequency. This indicates that nonlinear resonators can be utilized in designing acoustics diodes that can be operated at all wavelength limits.

Furthermore, we present the effect of nonlinear resonators in the image of 2-D fast Fourier transform depicted in Fig. 8. The linear signal is similar to the nonlinear signal as shown in Fig. 8.(a), thus confirming that the nonlinear chain has no effect in this limit. In Fig. 8.(b)-(c), the nonlinear resonator shows a wider distribution of the signal along both the frequency and wavenumber ranges in the long wavelength limit for both types of nonlinearity. This observation suggests that such nonlinear acoustic metamaterial can be suitable for applications such as acoustic diode. Fig. 8.(e) demonstrates that the nonlinear resonator is also effective in the short wavelength limit since it localizes the signal and stretches it over a wider region. Moreover, the results indicate that the energy content is concentrated in fixed slope dispersion curve unlike the case of linear chain. This is an indication that solitary localized waves can be observed at this wavelength limit with properly tuned hardening resonators. However, it is also demonstrated in Fig. 8.(d) and Fig. 8.(f) that the effect of nonlinear resonator vanishes when it is not tuned carefully. Overall, both spectral (wavenumber-frequency domain) and topological/physical (space-time domain) analyses provide good insight about the nonlinear effect on wave propagation

across all wavelength regions. But only the topological analysis can provide detail information about the physical features of wave propagation such as solitons formation.

Finally, we check the limitation of our analytical solution in weakly nonlinear systems for nonlinearity in the chain and the resonator. In Fig. 9, we plot the analytical solution for the linear and nonlinear dispersion curves against the images of 2D FFT for the numerical simulations. For the nonlinear chain case, our solution shows a good agreement with the numerical results for small value of nonlinearity ($\epsilon\bar{\Gamma} \leq 0.06$) as shown in Fig. 9 (a). The figure also indicates that the solitary nonlinear component with high energy content (shown in Fig. 8 (e)) coincides with the nonlinear dispersion curve while the linear component with low energy content coincides with the linear dispersion curves. Increasing the nonlinearity further ($\epsilon\bar{\Gamma} \geq 0.06$) gives rise to a new component between the linear and nonlinear dispersion curves in addition to the previously observed linear and nonlinear components. Nevertheless, the nonlinear component still coincides with the nonlinear dispersion curves, which indicates that the analytical solution is still accurate in terms of the bandgap boundaries. This new component has a fixed slope with energy content lower than the energy content of the main nonlinear component. Yet its energy content increases with increasing nonlinearity. However, for values beyond ($\epsilon\bar{\Gamma} \geq 0.15$), a discrepancy between the analytical and numerical solutions can be observed although the main numerical nonlinear component is still closer to the analytical nonlinear dispersion curve than the linear dispersion curves as shown in Fig. 9 (c). Moreover, the

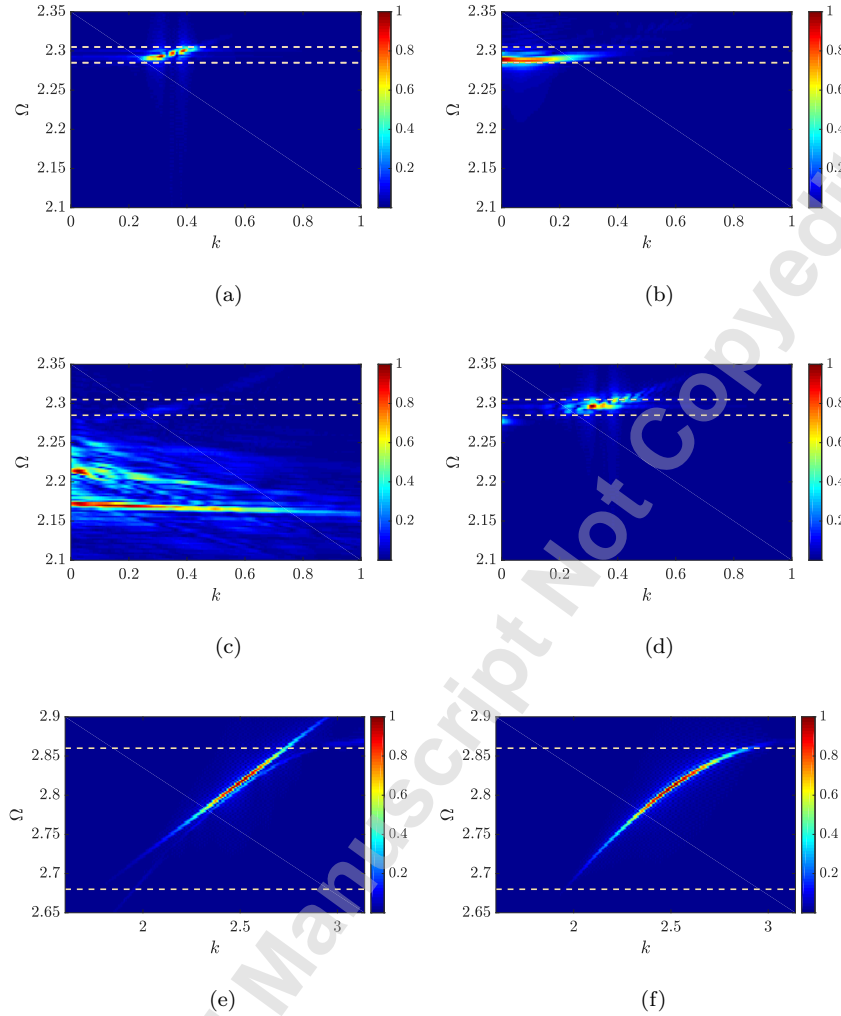


Figure 8: 2-D Fourier transform of the response for different types and sources of nonlinearities at frequencies in the upper branch of dispersion curve: (a) Hardening chain nonlinearity $\epsilon\bar{\Gamma}\alpha^2 = 0.03$, $\epsilon\bar{\Gamma}_1\alpha^2 = \epsilon\bar{\Gamma}_2\alpha^2 = 0$, $k = \pi/9$; (b) Hardening resonator nonlinearity $\epsilon\bar{\Gamma}_2\alpha^2 = 0.03$, $\epsilon\bar{\Gamma}_1\alpha^2 = \epsilon\bar{\Gamma}\alpha^2 = 0$, $k = \pi/9$; (c) Softening resonator nonlinearity $\epsilon\bar{\Gamma}_2\alpha^2 = -0.03$, $\epsilon\bar{\Gamma}_1\alpha^2 = \epsilon\bar{\Gamma}\alpha^2 = 0$, $k = \pi/9$; (d) Hardening resonator nonlinearity $\epsilon\bar{\Gamma}_1\alpha^2 = 0.03$, $\epsilon\bar{\Gamma}_2\alpha^2 = \epsilon\bar{\Gamma}\alpha^2 = 0$, $k = \pi/9$; (e) Hardening resonator nonlinearity $\epsilon\bar{\Gamma}_2\alpha^2 = 0.03$, $\epsilon\bar{\Gamma}_1\alpha^2 = \epsilon\bar{\Gamma}\alpha^2 = 0$, $k = 7\pi/9$; (f) Hardening resonator nonlinearity $\epsilon\bar{\Gamma}_1\alpha^2 = 0.03$, $\epsilon\bar{\Gamma}_2\alpha^2 = \epsilon\bar{\Gamma}\alpha^2 = 0$, $k = 7\pi/9$. Dashed lines represents linear frequency bands.

new component is more dominant and has higher energy content due to the increase of nonlinearity. For the nonlinear resonator case, Fig. 9 (d) demonstrates that the analytical solution fails to predict the nonlinear dispersion curve at frequencies close to the nonlinear resonator frequency and the numerical results completely coincide with the analytical linear dispersion curve instead of the nonlinear dispersion curve. However, at frequencies away from the nonlinear resonator frequency, the analytical solution can accurately predict the numerical results for small values of nonlinearity ($\epsilon\bar{\Gamma} < 0.15$) as shown in Fig. 9 (e). Beyond that both solutions start departing from each other as shown in Fig. 9 (f) and the analytical solution does not predict the actual dispersion curves accurately.

6. COMPUTATIONAL STUDY USING ANSYS APDL

In order to further validate and demonstrate the analytical bandgaps and the interesting nonlinear wave propagation phenomena obtained by the theoretical analysis, we conduct a computational study using finite element software, ANSYS. This computational analysis is based on a long nonlinear chain with linear resonator, as well as, a long linear chain with nonlinear resonator.

The geometry of the metamaterials is first created by a group of nodes and elements in the preprocessor section of ANSYS Parametric Design Language (APDL). The number of nodes is equal to the number of cells. Three types of elements are defined as: COMBIN14 for the stiffness of the linear spring, MASS21 for the mass of the chain and resonator, and COMBIN39 for the stiff-

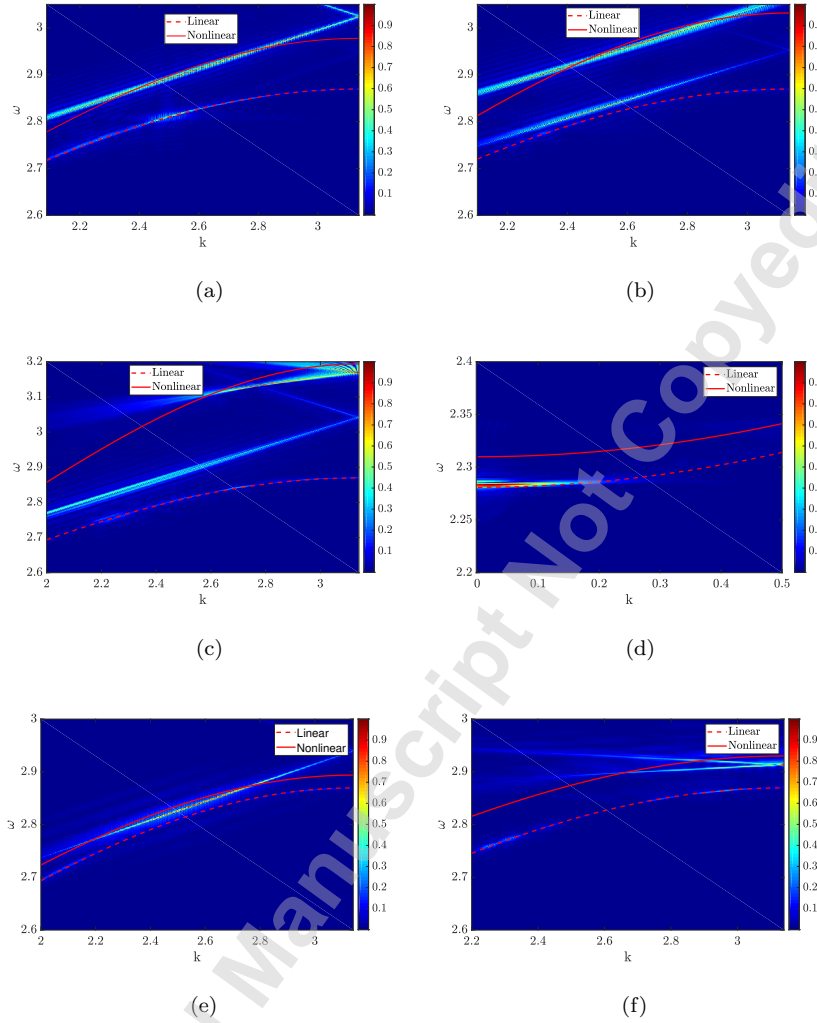


Figure 9: Comparison between the analytical solution and images of 2D FFT of the numerical simulations for a chain with two resonators: (a) Hardening chain nonlinearity $\epsilon\bar{\Gamma}\alpha^2 = 0.06$, $\epsilon\bar{\Gamma}_1\alpha^2 = \epsilon\bar{\Gamma}_2\alpha^2 = 0$, $k = 7\pi/9$; (b) Hardening chain nonlinearity $\epsilon\bar{\Gamma}\alpha^2 = 0.09$, $\epsilon\bar{\Gamma}_1\alpha^2 = \epsilon\bar{\Gamma}_2\alpha^2 = 0$, $k = 7\pi/9$; (c) Hardening chain nonlinearity $\epsilon\bar{\Gamma}\alpha^2 = 0.18$, $\epsilon\bar{\Gamma}_1\alpha^2 = \epsilon\bar{\Gamma}_2\alpha^2 = 0$, $k = 7\pi/9$; (d) Hardening resonator nonlinearity $\epsilon\bar{\Gamma}_2\alpha^2 = 0.03$, $\epsilon\bar{\Gamma}_1\alpha^2 = \epsilon\bar{\Gamma}\alpha^2 = 0$, $k = \pi/9$; (e) Hardening resonator nonlinearity $\epsilon\bar{\Gamma}_2\alpha^2 = 0.06$, $\epsilon\bar{\Gamma}_1\alpha^2 = \epsilon\bar{\Gamma}\alpha^2 = 0$, $k = 7\pi/9$; (f) Hardening resonator nonlinearity $\epsilon\bar{\Gamma}_2\alpha^2 = 0.15$, $\epsilon\bar{\Gamma}_1\alpha^2 = \epsilon\bar{\Gamma}\alpha^2 = 0$, $k = 7\pi/9$.

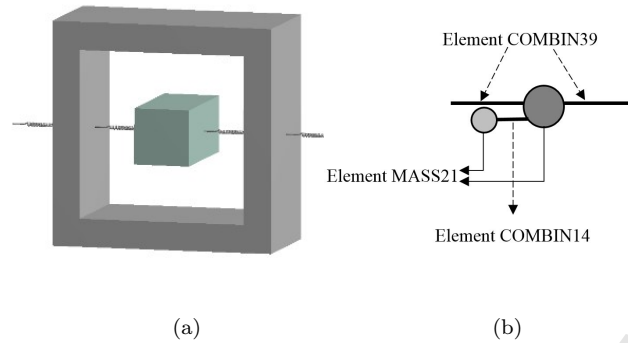


Figure 10: (a) A schematic of a cell in ANSYS Workbench; (b) equivalent diagram in APDL.

ness of the nonlinear spring. The values of the linear spring and mass are assigned to their elements by command “R”. For the nonlinear spring (in the nonlinear chain or the nonlinear resonator cases), we define the weak nonlinearity by a force-displacement curve. These values were then assigned to the element COMBIN39 by command “R”.

Each rigid chain and resonator is created by one node using commands “N” and “*REPEAT”. Next, element MASS21 is assigned to its corresponding node using commands “TYPE” and “REAL”. Fig. 10 shows the schematic of a cell in ANSYS workbench (Fig. 10. (a)) and its equivalent diagram in ANSYS APDL (Fig. 10. (b)). In Fig. 10.(a), two linear springs each with a stiffness of $k_1/2$ connect in parallel the chain to the resonator. These two springs are merged into one element defined as COMBIN14 with an equivalent stiffness of k_1 .

6.1. Band Structures

In order to determine the passband and bandgap, we excite the metamaterial by a harmonic force and monitor the output amplitude at each frequency in the frequency sweep range. Following [39], we excite the second chain in the metamaterial and record the response of the last cell of the chain at the other end.

For the single resonator case, we plot the frequency response curve for different sources of nonlinearities in Fig. 11. (a)-(c). In Fig. 11. (a)-(b), the results indicate that the wave does not propagate through the structure for frequencies inside the bandgap in the linear and nonlinear chain cases. These frequency limits show a very good agreement with those obtained analytically (marked by the dashed lines in Fig. 11). Moreover, the results demonstrate that both methods (i.e., computational and analytical) can capture the shift in the bandgap boundaries due to the nonlinearity in the chain. On the other hand, the wave propagates in the passband (outside the bandgap) since the amplitude of the system is much higher as compared to the amplitude inside the bandgap. However, for the nonlinear resonator case (Fig. 11. (c)), the results indicate that our analytical solution over estimates the bandgap boundaries. This error in bandgap appears mainly close to the nonlinear resonator frequency within the end of the acoustics branch and at the beginning of the optical branch.

For the case of two resonators, we plot the frequency response curve of the system for different types of nonlinearities in Fig. 11 (d)-(f). The computational results obtained by ANSYS reveal a good agreement with the analytical solution

for the linear and nonlinear chain cases as shown in Fig. 11 (d)-(e). However, the analytical results fails again in matching the computational results for the nonlinear resonator case, especially at the nonlinear resonator frequencies, as shown in Fig. 11. (f). The different regions (i.e., passband and bandgap) between the dashed lines separate the regions of high amplitude response and the zero amplitude response in the system.

6.2. Spectro-Spatial Analysis of ANSYS Results

In this section, we demonstrate the presence of solitary waves based on ANSYS computational simulations. We excite the chain by a wave packet and plot the spatial profile of the output wave, the spectrograms of the wave propagation, and the 2DFFT images in Figs. 12- 14.

For the spatial profile, we observe that a nonlinear chain has no effect on the wave profile at long wavelength limit while the nonlinear resonator distorts the signal significantly as shown in Fig. 12. (a). This distortion can lead to a significant frequency shift (i.e., the output signal appears at frequencies different than the frequency of the input signal) and shows a good agreement with the theoretical results obtained in the previous section. The wave profile for the linear chain is a mirror image of the nonlinear chain case. On the other hand, in Fig. 12. (b), the nonlinearity in the chain and resonator shows a birth of localized solitary waves at short wavelength limit and the profile of the linear chain is different from that of the nonlinear chain since it is completely dispersive. These findings were also observed in the numerical analysis in the previous section, except that in the computational simulation the localized component in

the nonlinear resonator case is not sharp as compared to the numerical results.

In Fig. 13 (a)-(b), spatial spectrograms further demonstrate the wave distortion and wave number/frequency shift due to the nonlinear resonator at long wavelength limit. In particular, some of the energy content for the output signal appears outside the input wavenumber/frequency band as shown in Fig. 13 (b). This distortion cannot be obtained in the nonlinear chain case (Fig. 13 (a)) since its spectrogram is a mirror image of the linear chain case. On the other hand, the spatial spectrogram plots in Fig. 13 (c)-(d) indicate that all energy content of the output wave is concentrated in one component inside the input wavenumber/frequency band with high energy. This observation suggests the birth of localized wave at short wavelength limit. Although, the wave in Fig. 13 (d) looks dispersive, the wave still has localized component that preserves high energy content.

Finally, we show the images of 2DFFT in Fig. 14 to demonstrate the effect of nonlinearity on the dispersion curve based on the results obtained in ANSYS. In the long wavelength limit, the results indicate that the nonlinearity in the chain does not distort the wave since its profile (shown in Fig. 13 (a)) is exactly the same as the profile of the linear chain. On the other hand, the nonlinearity in the resonator distorts the output wave since the wave (Fig. 14. (b)) appears at frequency different than the input frequency which is identical to the undistorted wave of the linear and nonlinear chain shown in Fig. 13 (a). In the short wavelength limit, the image of the nonlinear chain (Fig. 14. (c)) shows that the energy content of the output wave appears on two main components.

One with variable slope and coincides with the linear dispersion curve, the other has fixed slope and appears above the linear dispersion curve due to the type of hardening nonlinearity. The latter represents a solitary wave [23]. For the nonlinear resonator case (Fig. 14. (d)), distinguishing the two energy components is harder since this region is not affected by the resonator nonlinearity as compared to the nonlinear chain. Yet the hardening resonator nonlinearity shifts the dispersion curves up toward the fixed slope case which indicates the birth of solitary wave.

7. CONCLUSION

In this paper, a nonlinear acoustics metamaterial with multiple local resonators was investigated theoretically and computationally. In one case, we examined the nonlinearity in the chains and in another we investigated the nonlinearity in the resonators. Closed-form expressions were presented for the nonlinear dispersion relations using the method of multiple scales. These expressions are more general since they can be applied for nonlinear chains with any number of nonlinear local resonators. The analytical results were validated via comparison with those in the literature, those obtained numerically, and those obtained by finite element software, ANSYS. The validation revealed that the analytical results can predict the cut-off frequency in both cases; however, the analytical approach fails to predict the dispersion curve near the resonator frequency. This failure suggests that higher perturbation or more robust analytical techniques may be required to accurately predict the dispersion relations of such

a nonlinear metastructure. The analytical dispersion equation for the case of nonlinear resonator shows a significant frequency shift at all wavelength limits, particularly when the excitation frequency is near the resonator frequency. This finding is an indication that nonlinear resonators in the present system, unlike nonlinear chains, affect wave propagations in the long wavelength domain. This observation was consistent with the topological (space-time domain) analysis conducted based on numerical and computational simulations. In the spectro-spatial analysis, we demonstrated that the effect of hardening nonlinearity appears as localizing the wave, whereas, that of softening nonlinearity appears as dispersing the wave. This effect depends on the nonlinear resonator frequency and how close it is to the input wave frequency. Spectrograms and images of 2-D short term Fourier transform also confirmed these observations. They also showed that the nonlinear resonator has output signal stretching over a wider range of frequencies and wavenumbers in the long wavelength region. In addition, the nonlinear resonators and nonlinear chains exhibited similar waveform characteristics in short wavelength region when the nonlinear resonator was tuned properly. These observations suggest that such a nonlinear metamaterial (i.e, metamaterial investigated in the current study), consisting of a nonlinear (or linear) chain and multiple linear (or nonlinear) resonators, are suitable for various applications including acoustic diodes and broadband vibration isolation and energy harvesting. The current findings can be further supported or generalized upon investigating similar systems using various analytical and experimental techniques and employing these observations in various applications

like acoustics diode in the future.

acknowledgment

This work was supported by the start-up grant provided by the Department of Mechanical Engineering at Virginia Tech.

References

- [1] M. I. Hussein, M. J. Leamy, M. Ruzzene, Dynamics of phononic materials and structures: Historical origins, recent progress, and future outlook, *Applied Mechanics Reviews* 66 (4) (2014) 040802.
- [2] K. Bertoldi, V. Vitelli, J. Christensen, M. van Hecke, Flexible mechanical metamaterials, *Nature Reviews Materials* 2 (11) (2017) 17066.
- [3] M. M. Sigalas, E. N. Economou, Elastic and acoustic wave band structure, *Journal of Sound Vibration* 158 (1992) 377–382.
- [4] M. Sigalas, E. N. Economou, Band structure of elastic waves in two dimensional systems, *Solid state communications* 86 (3) (1993) 141–143.
- [5] M. S. Kushwaha, P. Halevi, L. Dobrzynski, B. Djafari-Rouhani, Acoustic band structure of periodic elastic composites, *Physical review letters* 71 (13) (1993) 2022.
- [6] M. S. Kushwaha, P. Halevi, G. Martinez, L. Dobrzynski, B. Djafari-Rouhani, Theory of acoustic band structure of periodic elastic composites, *Physical Review B* 49 (4) (1994) 2313.

-
- [7] J. Vasseur, B. Djafari-Rouhani, L. Dobrzynski, M. Kushwaha, P. Halevi, Complete acoustic band gaps in periodic fibre reinforced composite materials: the carbon/epoxy composite and some metallic systems, *Journal of Physics: Condensed Matter* 6 (42) (1994) 8759.
- [8] M. S. Kushwaha, Classical band structure of periodic elastic composites, *International Journal of Modern Physics B* 10 (09) (1996) 977–1094.
- [9] Z. Liu, X. Zhang, Y. Mao, Y. Zhu, Z. Yang, C. T. Chan, P. Sheng, Locally resonant sonic materials, *science* 289 (5485) (2000) 1734–1736.
- [10] L. Liu, M. I. Hussein, Wave motion in periodic flexural beams and characterization of the transition between bragg scattering and local resonance, *Journal of Applied Mechanics* 79 (1) (2012) 011003.
- [11] G. Huang, C. Sun, Band gaps in a multiresonator acoustic metamaterial, *Journal of Vibration and Acoustics* 132 (3) (2010) 031003.
- [12] R. Zhu, X. Liu, G. Hu, C. Sun, G. Huang, A chiral elastic metamaterial beam for broadband vibration suppression, *Journal of Sound and Vibration* 333 (10) (2014) 2759–2773.
- [13] Y. S. Kivshar, N. Flytzanis, Gap solitons in diatomic lattices, *Physical Review A* 46 (12) (1992) 7972.
- [14] N. Nadkarni, C. Daraio, D. M. Kochmann, Dynamics of periodic mechanical structures containing bistable elastic elements: From elastic to solitary wave propagation, *Physical Review E* 90 (2) (2014) 023204.

-
- [15] B. Liang, B. Yuan, J.-c. Cheng, Acoustic diode: Rectification of acoustic energy flux in one-dimensional systems, *Physical review letters* 103 (10) (2009) 104301.
- [16] J. M. Manimala, C. Sun, Numerical investigation of amplitude-dependent dynamic response in acoustic metamaterials with nonlinear oscillators, *The Journal of the Acoustical Society of America* 139 (6) (2016) 3365–3372.
- [17] A. H. Nayfeh, *Introduction to perturbation techniques*, John Wiley & Sons, 2011.
- [18] A. H. Nayfeh, D. T. Mook, *Nonlinear oscillations*, John Wiley & Sons, 2008.
- [19] R. K. Narisetti, M. J. Leamy, M. Ruzzene, A perturbation approach for predicting wave propagation in one-dimensional nonlinear periodic structures, *Journal of Vibration and Acoustics* 132 (3) (2010) 031001.
- [20] K. Manktelow, M. J. Leamy, M. Ruzzene, Multiple scales analysis of wave-wave interactions in a cubically nonlinear monoatomic chain, *Nonlinear Dynamics* 63 (1-2) (2011) 193–203.
- [21] B. S. Lazarov, J. S. Jensen, Low-frequency band gaps in chains with attached non-linear oscillators, *International Journal of Non-Linear Mechanics* 42 (10) (2007) 1186–1193.
- [22] R. Khajehtourian, M. I. Hussein, Dispersion characteristics of a nonlinear elastic metamaterial, *Aip Advances* 4 (12) (2014) 124308.

-
- [23] M. Hussein, R. Khajehtourian, Nonlinear bloch waves and balance between hardening and softening dispersion, *Proceedings of the Royal Society A: Mathematical, Physical and Engineering Sciences* 474 (2217) (2018) 20180173.
- [24] X. Fang, J. Wen, H. Benisty, D. Yu, Ultrabroad acoustical limiting in nonlinear metamaterials due to adaptive-broadening band-gap effect, *Physical Review B* 101 (10) (2020) 104304.
- [25] X. Xu, M. V. Barnhart, X. Fang, J. Wen, Y. Chen, G. Huang, A nonlinear dissipative elastic metamaterial for broadband wave mitigation, *International Journal of Mechanical Sciences* 164 (2019) 105159.
- [26] B. Liang, X. Guo, J. Tu, D. Zhang, J. Cheng, An acoustic rectifier, *Nature materials* 9 (12) (2010) 989.
- [27] X.-F. Li, X. Ni, L. Feng, M.-H. Lu, C. He, Y.-F. Chen, Tunable unidirectional sound propagation through a sonic-crystal-based acoustic diode, *Physical review letters* 106 (8) (2011) 084301.
- [28] N. Boechler, G. Theocharis, C. Daraio, Bifurcation-based acoustic switching and rectification, *Nature materials* 10 (9) (2011) 665.
- [29] K. J. Moore, J. Bunyan, S. Tawfick, O. V. Gendelman, S. Li, M. Leamy, A. F. Vakakis, Nonreciprocity in the dynamics of coupled oscillators with nonlinearity, asymmetry, and scale hierarchy, *Physical Review E* 97 (1) (2018) 012219.

-
- [30] C. Ma, R. G. Parker, B. B. Yellen, Optimization of an acoustic rectifier for uni-directional wave propagation in periodic mass–spring lattices, *Journal of Sound and Vibration* 332 (20) (2013) 4876–4894.
- [31] R. Ganesh, S. Gonella, Spectro-spatial wave features as detectors and classifiers of nonlinearity in periodic chains, *Wave Motion* 50 (4) (2013) 821–835.
- [32] W. Zhou, X. Li, Y. Wang, W. Chen, G. Huang, Spectro-spatial analysis of wave packet propagation in nonlinear acoustic metamaterials, *Journal of Sound and Vibration* 413 (2018) 250–269.
- [33] M. Bukhari, O. Barry, Nonlinear metamaterials with multiple local mechanical resonators: Analytical and numerical analyses, in: *New Trends in Nonlinear Dynamics*, Springer, 2020, pp. 13–21.
- [34] M. Bukhari, O. Barry, Spectro-spatial analyses of a nonlinear metamaterial with multiple nonlinear local resonators, *Nonlinear Dynamics* (2019) 1–22.
- [35] M. A. Bukhari, O. R. Barry, On the spectro-spatial wave features in nonlinear metamaterials with multiple local resonators, in: *ASME 2019 International Design Engineering Technical Conferences and Computers and Information in Engineering Conference*, Anaheim, CA, August 2019, American Society of Mechanical Engineers Digital Collection, 2019.
- [36] F. Bloch, Über die quantenmechanik der elektronen in kristallgittern, *Zeitschrift für physik* 52 (7-8) (1929) 555–600.
- [37] G. Floquet, Sur les équations différentielles linéaires à coefficients

périodiques, in: Annales scientifiques de l'École normale supérieure, Vol. 12, 1883, pp. 47-88.

[38] J. M. Manimala, Dynamic behavior of acoustic metamaterials and meta-configured structures with local oscillators, Ph.D. thesis, Purdue University (2014).

[39] G. Hu, L. Tang, R. Das, Internally coupled metamaterial beam for simultaneous vibration suppression and low frequency energy harvesting, Journal of Applied Physics 123 (5) (2018) 055107.

List of Figures

1	A schematic diagram for the nonlinear acoustics metamaterial . . .	3
2	Validating the results of nonlinear chain with single linear resonator, $\epsilon\bar{\Gamma}\alpha^2 = 0.06$, $\epsilon\bar{\Gamma}_1\alpha^2 = 0$	11
3	Validating the results of nonlinear chain with two linear resonators, $\epsilon\bar{\Gamma}\alpha^2 = 0.06$, $\epsilon\bar{\Gamma}_1\alpha^2 = \epsilon\bar{\Gamma}_2\alpha^2 = 0$	11
4	Validating the results of linear chain with two nonlinear resonators, $\epsilon\bar{\Gamma}\alpha^2 = 0$, $\epsilon\bar{\Gamma}_1\alpha^2 = 0.06$, $\epsilon\bar{\Gamma}_2\alpha^2 = 0$	12

-
- 5 Analytical dispersion curves for acoustics metamaterial and two local resonators with different types and sources of nonlinearities:
 (a) Softening chain nonlinearity $\epsilon\bar{\Gamma}\alpha^2 = -0.06$, $\epsilon\bar{\Gamma}_1\alpha^2 = \epsilon\bar{\Gamma}_2\alpha^2 = 0$; (b) Hardening resonator nonlinearity $\epsilon\bar{\Gamma}_2\alpha^2 = 0.06$, $\epsilon\bar{\Gamma}_1\alpha^2 = \epsilon\bar{\Gamma}\alpha^2 = 0$; (c) Softening resonator nonlinearity $\epsilon\bar{\Gamma}_1\alpha^2 = -0.06$, $\epsilon\bar{\Gamma}\alpha^2 = \epsilon\bar{\Gamma}_2\alpha^2 = 0$; (d) Softening resonator nonlinearity $\epsilon\bar{\Gamma}_2\alpha^2 = -0.06$, $\epsilon\bar{\Gamma}_1\alpha^2 = \epsilon\bar{\Gamma}\alpha^2 = 0$ 13
- 6 Spatial profile of the wave packet for different types and sources of nonlinearities at frequencies in the upper branch of dispersion curve: (a) Linear chain $\epsilon\bar{\Gamma}\alpha^2 = \epsilon\bar{\Gamma}_1\alpha^2 = \epsilon\bar{\Gamma}_2\alpha^2 = 0$; (b) Hardening chain nonlinearity $\epsilon\bar{\Gamma}\alpha^2 = 0.03$, $\epsilon\bar{\Gamma}_1\alpha^2 = \epsilon\bar{\Gamma}_2\alpha^2 = 0$; (c) Softening chain nonlinearity $\epsilon\bar{\Gamma}\alpha^2 = -0.03$, $\epsilon\bar{\Gamma}_1\alpha^2 = \epsilon\bar{\Gamma}_2\alpha^2 = 0$; (d) Hardening resonator nonlinearity $\epsilon\bar{\Gamma}_2\alpha^2 = 0.03$, $\epsilon\bar{\Gamma}_1\alpha^2 = \epsilon\bar{\Gamma}\alpha^2 = 0$; (e) Softening resonator nonlinearity $\epsilon\bar{\Gamma}_2\alpha^2 = -0.03$, $\epsilon\bar{\Gamma}_1\alpha^2 = \epsilon\bar{\Gamma}\alpha^2 = 0$; (f) Hardening resonator nonlinearity $\epsilon\bar{\Gamma}_1\alpha^2 = 0.03$, $\epsilon\bar{\Gamma}_2\alpha^2 = \epsilon\bar{\Gamma}\alpha^2 = 0$ 14

Accepted Manuscript

- 7 Spatial spectrograms of the wave packet for different types and sources of nonlinearities at frequencies in the upper branch of dispersion curve: (a) Hardening chain nonlinearity $\epsilon\bar{\Gamma}\alpha^2 = 0.03$, $\epsilon\bar{\Gamma}_1\alpha^2 = \epsilon\bar{\Gamma}_2\alpha^2 = 0$, $k = \pi/9$; (b) Hardening resonator nonlinearity $\epsilon\bar{\Gamma}_2\alpha^2 = 0.03$, $\epsilon\bar{\Gamma}_1\alpha^2 = \epsilon\bar{\Gamma}\alpha^2 = 0$, $k = \pi/9$; (c) Softening resonator nonlinearity $\epsilon\bar{\Gamma}_2\alpha^2 = -0.03$, $\epsilon\bar{\Gamma}_1\alpha^2 = \epsilon\bar{\Gamma}\alpha^2 = 0$, $k = \pi/9$; (d) Hardening resonator nonlinearity $\epsilon\bar{\Gamma}_1\alpha^2 = 0.03$, $\epsilon\bar{\Gamma}_2\alpha^2 = \epsilon\bar{\Gamma}\alpha^2 = 0$, $k = \pi/9$; (e) Hardening resonator nonlinearity $\epsilon\bar{\Gamma}_2\alpha^2 = 0.03$, $\epsilon\bar{\Gamma}_1\alpha^2 = \epsilon\bar{\Gamma}\alpha^2 = 0$, $k = 7\pi/9$; (f) Hardening resonator nonlinearity $\epsilon\bar{\Gamma}_1\alpha^2 = 0.03$, $\epsilon\bar{\Gamma}_2\alpha^2 = \epsilon\bar{\Gamma}\alpha^2 = 0$, $k = 7\pi/9$. 15
- 8 2-D Fourier transform of the response for different types and sources of nonlinearities at frequencies in the upper branch of dispersion curve: (a) Hardening chain nonlinearity $\epsilon\bar{\Gamma}\alpha^2 = 0.03$, $\epsilon\bar{\Gamma}_1\alpha^2 = \epsilon\bar{\Gamma}_2\alpha^2 = 0$, $k = \pi/9$; (b) Hardening resonator nonlinearity $\epsilon\bar{\Gamma}_2\alpha^2 = 0.03$, $\epsilon\bar{\Gamma}_1\alpha^2 = \epsilon\bar{\Gamma}\alpha^2 = 0$, $k = \pi/9$; (c) Softening resonator nonlinearity $\epsilon\bar{\Gamma}_2\alpha^2 = -0.03$, $\epsilon\bar{\Gamma}_1\alpha^2 = \epsilon\bar{\Gamma}\alpha^2 = 0$, $k = \pi/9$; (d) Hardening resonator nonlinearity $\epsilon\bar{\Gamma}_1\alpha^2 = 0.03$, $\epsilon\bar{\Gamma}_2\alpha^2 = \epsilon\bar{\Gamma}\alpha^2 = 0$, $k = \pi/9$; (e) Hardening resonator nonlinearity $\epsilon\bar{\Gamma}_2\alpha^2 = 0.03$, $\epsilon\bar{\Gamma}_1\alpha^2 = \epsilon\bar{\Gamma}\alpha^2 = 0$, $k = 7\pi/9$; (f) Hardening resonator nonlinearity $\epsilon\bar{\Gamma}_1\alpha^2 = 0.03$, $\epsilon\bar{\Gamma}_2\alpha^2 = \epsilon\bar{\Gamma}\alpha^2 = 0$, $k = 7\pi/9$. Dashed lines represents linear frequency bands. . . . 23

9	Comparison between the analytical solution and images of 2D FFT of the numerical simulations for a chain with two resonators: (a) Hardening chain nonlinearity $\epsilon\bar{\Gamma}\alpha^2 = 0.06$, $\epsilon\bar{\Gamma}_1\alpha^2 = \epsilon\bar{\Gamma}_2\alpha^2 = 0$, $k = 7\pi/9$; (b) Hardening chain nonlinearity $\epsilon\bar{\Gamma}\alpha^2 = 0.09$, $\epsilon\bar{\Gamma}_1\alpha^2 = \epsilon\bar{\Gamma}_2\alpha^2 = 0$, $k = 7\pi/9$; (c) Hardening chain nonlinearity $\epsilon\bar{\Gamma}\alpha^2 = 0.18$, $\epsilon\bar{\Gamma}_1\alpha^2 = \epsilon\bar{\Gamma}_2\alpha^2 = 0$, $k = 7\pi/9$; (d) Hardening resonator nonlinearity $\epsilon\bar{\Gamma}_2\alpha^2 = 0.03$, $\epsilon\bar{\Gamma}_1\alpha^2 = \epsilon\bar{\Gamma}\alpha^2 = 0$, $k = \pi/9$; (e) Hardening resonator nonlinearity $\epsilon\bar{\Gamma}_2\alpha^2 = 0.06$, $\epsilon\bar{\Gamma}_1\alpha^2 = \epsilon\bar{\Gamma}\alpha^2 = 0$, $k = 7\pi/9$; (f) Hardening resonator nonlinearity $\epsilon\bar{\Gamma}_2\alpha^2 = 0.15$, $\epsilon\bar{\Gamma}_1\alpha^2 = \epsilon\bar{\Gamma}\alpha^2 = 0$, $k = 7\pi/9$	25
10	(a) A schematic of a cell in ANSYS Workbench; (b) equivalent diagram in APDL.	26
11	Frequency response curves for a linear and nonlinear metamaterial with marking the boundaries of the analytical bandgaps by dashed lines: (a) Linear chain single resonator $\epsilon\bar{\Gamma}\alpha^2 = \epsilon\bar{\Gamma}_1\alpha^2 = 0$; (b) Nonlinear chain single resonator $\epsilon\bar{\Gamma}\alpha^2 = 0.06$; $\epsilon\bar{\Gamma}_1\alpha^2 = 0$; (c) Nonlinear resonator single resonator $\epsilon\bar{\Gamma}\alpha^2 = 0$; $\epsilon\bar{\Gamma}_1\alpha^2 = 0.06$; (d) Linear chain two resonators $\epsilon\bar{\Gamma}\alpha^2 = \epsilon\bar{\Gamma}_1\alpha^2 = \epsilon\bar{\Gamma}_2\alpha^2 = 0$; (e) Nonlinear chain two resonators $\epsilon\bar{\Gamma}\alpha^2 = 0.06$; $\epsilon\bar{\Gamma}_1\alpha^2 = \epsilon\bar{\Gamma}_2\alpha^2 = 0$; Nonlinear resonator two resonators $\epsilon\bar{\Gamma}\alpha^2 = \epsilon\bar{\Gamma}_2\alpha^2 = 0$; $\epsilon\bar{\Gamma}_1\alpha^2 = 0.06$	42

-
- 12 Spatial profile in short and long wavelength limits in the upper optical mode (a chain with two resonators) for linear chain, nonlinear chain, and nonlinear resonator: (a) $k = \pi/9$; (b) $k = 7\pi/9$. 43
- 13 Spatial spectrograms for nonlinear metamaterial with two local resonators in short and long wavelength limits: (a) Nonlinear chain, $\epsilon\bar{\Gamma}\alpha^2 = 0.03$, $\epsilon\bar{\Gamma}_1\alpha^2 = \epsilon\bar{\Gamma}_2\alpha^2 = 0$, $k = \pi/9$; (b) Nonlinear resonator, $\epsilon\bar{\Gamma}_2\alpha^2 = 0.03$, $\epsilon\bar{\Gamma}_1\alpha^2 = \epsilon\bar{\Gamma}\alpha^2 = 0$, $k = \pi/9$; (c) Nonlinear chain, $\epsilon\bar{\Gamma}\alpha^2 = 0.03$, $\epsilon\bar{\Gamma}_1\alpha^2 = \epsilon\bar{\Gamma}_2\alpha^2 = 0$, $k = 7\pi/9$; (d) Nonlinear resonator, $\epsilon\bar{\Gamma}_2\alpha^2 = 0.03$, $\epsilon\bar{\Gamma}_1\alpha^2 = \epsilon\bar{\Gamma}\alpha^2 = 0$, $k = 7\pi/9$. 44
- 14 Images of 2-D Fourier transform and nonlinear metamaterial with two local resonators in short and long wavelength limits : (a) Nonlinear chain, $\epsilon\bar{\Gamma}\alpha^2 = 0.03$, $\epsilon\bar{\Gamma}_1\alpha^2 = \epsilon\bar{\Gamma}_2\alpha^2 = 0$, $k = \pi/9$; (b) Nonlinear resonator, $\epsilon\bar{\Gamma}_2\alpha^2 = 0.03$, $\epsilon\bar{\Gamma}_1\alpha^2 = \epsilon\bar{\Gamma}\alpha^2 = 0$, $k = \pi/9$; (c) Nonlinear chain, $\epsilon\bar{\Gamma}\alpha^2 = 0.03$, $\epsilon\bar{\Gamma}_1\alpha^2 = \epsilon\bar{\Gamma}_2\alpha^2 = 0$, $k = 7\pi/9$; (d) Nonlinear resonator, $\epsilon\bar{\Gamma}_2\alpha^2 = 0.03$, $\epsilon\bar{\Gamma}_1\alpha^2 = \epsilon\bar{\Gamma}\alpha^2 = 0$, $k = 7\pi/9$ 45

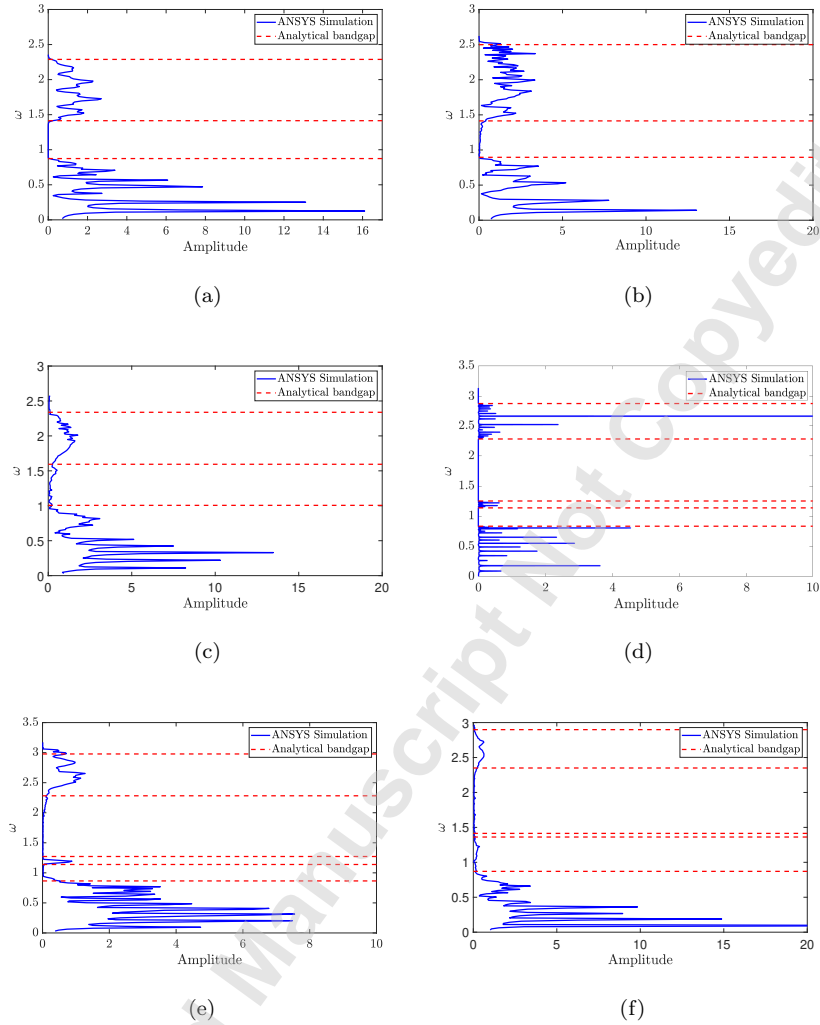


Figure 11: Frequency response curves for a linear and nonlinear metamaterial with marking the boundaries of the analytical bandgaps by dashed lines: (a) Linear chain single resonator $\epsilon\bar{\Gamma}\alpha^2 = \epsilon\bar{\Gamma}_1\alpha^2 = 0$; (b) Nonlinear chain single resonator $\epsilon\bar{\Gamma}\alpha^2 = 0.06$; $\epsilon\bar{\Gamma}_1\alpha^2 = 0$; (c) Nonlinear resonator single resonator $\epsilon\bar{\Gamma}\alpha^2 = 0$; $\epsilon\bar{\Gamma}_1\alpha^2 = 0.06$; (d) Linear chain two resonators $\epsilon\bar{\Gamma}\alpha^2 = \epsilon\bar{\Gamma}_1\alpha^2 = \epsilon\bar{\Gamma}_2\alpha^2 = 0$; (e) Nonlinear chain two resonators $\epsilon\bar{\Gamma}\alpha^2 = 0.06$; $\epsilon\bar{\Gamma}_1\alpha^2 = \epsilon\bar{\Gamma}_2\alpha^2 = 0$; Nonlinear resonator two resonators $\epsilon\bar{\Gamma}\alpha^2 = \epsilon\bar{\Gamma}_2\alpha^2 = 0$; $\epsilon\bar{\Gamma}_1\alpha^2 = 0.06$.

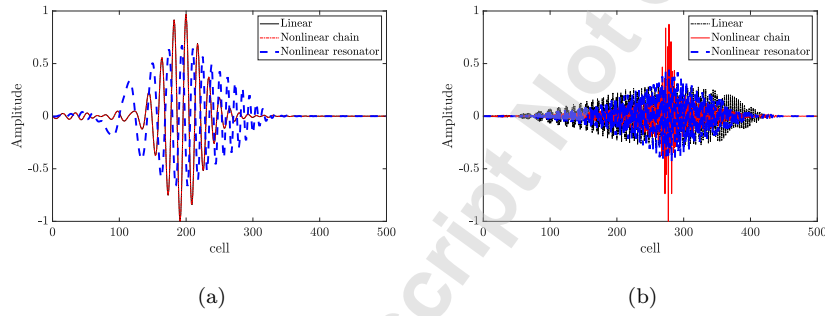


Figure 12: Spatial profile in short and long wavelength limits in the upper optical mode (a chain with two resonators) for linear chain, nonlinear chain, and nonlinear resonator: (a) $k = \pi/9$; (b) $k = 7\pi/9$.

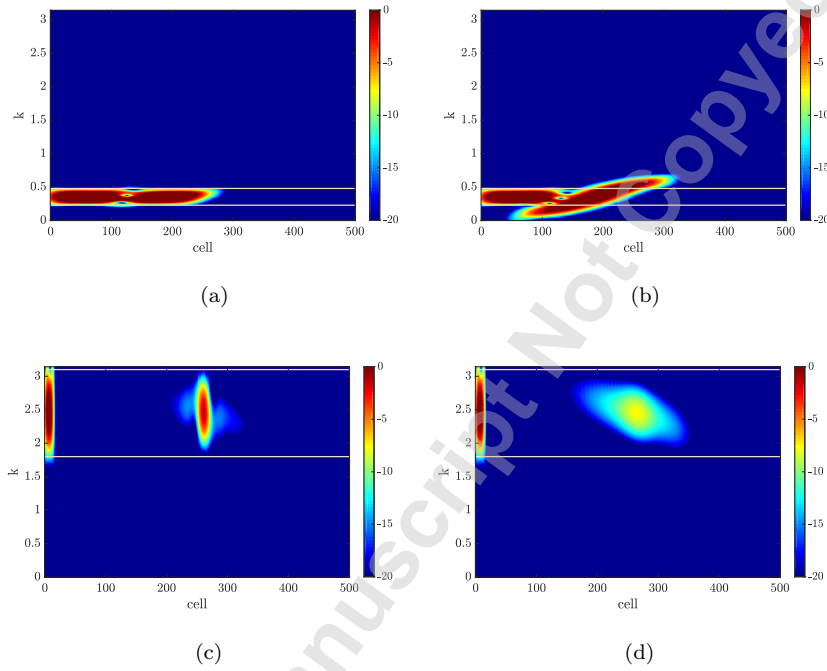


Figure 13: Spatial spectrograms for nonlinear metamaterial with two local resonators in short and long wavelength limits: (a) Nonlinear chain, $\epsilon\bar{\Gamma}\alpha^2 = 0.03$, $\epsilon\bar{\Gamma}_1\alpha^2 = \epsilon\bar{\Gamma}_2\alpha^2 = 0$, $k = \pi/9$; (b) Nonlinear resonator, $\epsilon\bar{\Gamma}_2\alpha^2 = 0.03$, $\epsilon\bar{\Gamma}_1\alpha^2 = \epsilon\bar{\Gamma}\alpha^2 = 0$, $k = \pi/9$; (c) Nonlinear chain, $\epsilon\bar{\Gamma}\alpha^2 = 0.03$, $\epsilon\bar{\Gamma}_1\alpha^2 = \epsilon\bar{\Gamma}_2\alpha^2 = 0$, $k = 7\pi/9$; (d) Nonlinear resonator, $\epsilon\bar{\Gamma}_2\alpha^2 = 0.03$, $\epsilon\bar{\Gamma}_1\alpha^2 = \epsilon\bar{\Gamma}\alpha^2 = 0$, $k = 7\pi/9$.

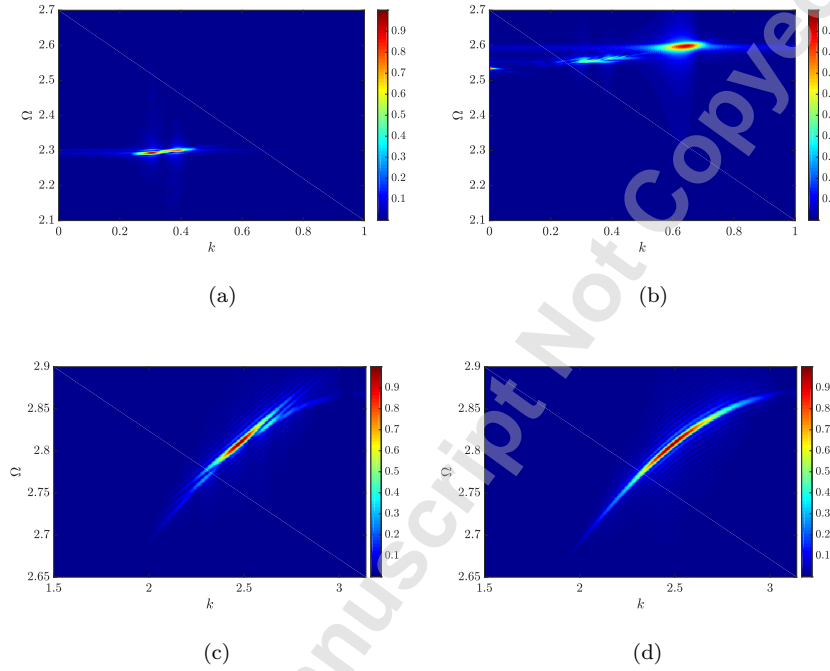


Figure 14: Images of 2-D Fourier transform and nonlinear metamaterial with two local resonators in short and long wavelength limits : (a) Nonlinear chain, $\epsilon\bar{\Gamma}\alpha^2 = 0.03$, $\epsilon\bar{\Gamma}_1\alpha^2 = \epsilon\bar{\Gamma}_2\alpha^2 = 0$, $k = \pi/9$; (b) Nonlinear resonator, $\epsilon\bar{\Gamma}_2\alpha^2 = 0.03$, $\epsilon\bar{\Gamma}_1\alpha^2 = \epsilon\bar{\Gamma}\alpha^2 = 0$, $k = \pi/9$; (c) Nonlinear chain, $\epsilon\bar{\Gamma}\alpha^2 = 0.03$, $\epsilon\bar{\Gamma}_1\alpha^2 = \epsilon\bar{\Gamma}_2\alpha^2 = 0$, $k = 7\pi/9$; (d) Nonlinear resonator, $\epsilon\bar{\Gamma}_2\alpha^2 = 0.03$, $\epsilon\bar{\Gamma}_1\alpha^2 = \epsilon\bar{\Gamma}\alpha^2 = 0$, $k = 7\pi/9$.